



1 **Singular spectrum and principal component analysis of soil radon**
2 **(Rn-222) emanation for better detection and correlation of seismic**
3 **induced anomalies**

4 Timangshu Chetia^{1,2}, Saurabh Baruah¹, Chandan Dey^{1,2}, Sangeeta Sharma¹, Santanu Baruah¹

5 ¹Geoscience & Technology Division, CSIR-North East Institute of Science and Technology
6 (CSIR-NEIST), Jorhat-785006, Assam, India

7 ²Academy of Scientific and Innovative Research (CSIR-NEIST), Jorhat-785006, Assam, India

8 *Correspondence to: Santanu Baruah (santanub27@gmail.com)

9

10 **Abstract.** In the recent years there are several reporting's of anomalous seismic induced
11 temporal changes in soil radon emanation. It is however well known that radon anomalies apart
12 from seismic activity are also governed and controlled by meteorological parameters. This is
13 the major complication which arise for isolating the seismic induced precursory signals. Here
14 in the investigation the soil radon emanations temporal variability at MPMO, Tezpur, is
15 scrutinized in the lime light of singular spectrum analysis (SSA). Further prior applying SSA
16 Digital filter (Butterworth low pass) is applied to remove the high frequency quasi periodic
17 component in the time series of soil radon emanation. It was scrutinized that sum of just 9
18 eigenfunctions were sufficient enough for reproducing the prominent characteristics of the
19 overall variation. This perhaps also evinces that more significantly produced fluctuations are
20 mostly free from natural variations. The variations in soil temperature was observed to be
21 dominated by daily variations similar to radon variation which account to 97.99 % whereas soil
22 pressure accounts for 100 % of the total variance which suggests that daily variations of soil
23 radon (Rn-222) emanation are controlled by soil pressure in MPMO, Tezpur during the
24 investigation period followed by soil temperature. The study concludes that SSA eliminates
25 diurnal and semidiurnal components from time series of soil radon emanation for better
26 correlation of soil radon emanation with earthquakes.



27 1 **Introduction**

28 Radon (Rn-222) is a noble gas, a decay product of radium with atomic number, $Z=86$
29 and a half-life of nearly 3.8 days. Because of its short decay time, amount changes in its
30 production from the rock is quite evidenced. Ulomov and Mavashev in the year 1971 (Ulomov
31 and Mavashev, 1971) first suggested the correlation of radon concentration with earthquakes.
32 It has been scrutinized that the radon concentration has correlation to earthquakes and volcanic
33 eruptions (Walia et al. 2006, Singh et al. 2005). Significant radon concentration anomalies were
34 also observed prior to the Uttarkashi earthquake of 20th October, 1991; $m_b \sim 6.5$ (Virk and Singh
35 1994). Radon concentrations was monitored in the North West Himalaya for earthquake
36 prediction studies and empirical equation between earthquake magnitude, epicentral distance
37 and precursory time were examined (Kumar et al. 2009). Earthquake prediction depending
38 entirely on precursory phenomena is empirical and comprises many applied problems. Among
39 various geophysical parameters soil radon is preferred and used for earthquake precursory
40 studies because of its ease of detectability. Radon in nature has different isotopes: Rn-222 (half-
41 life~3.8 days), Rn-220 (Thoron, half-life~54.5 s) and Rn-219 (half-life~3.92 s). The utmost
42 prominent is Rn-222 because of its longer half-life which is a product of Ra-226 decay process.
43 The Rn-222 emanates from soil or crust either by diffusion or convection and reaches the
44 atmosphere. The soil radon emanation concentration is generally assigned to developments of
45 micro-cracks, fissure and fracture due to dilatancy prior to earthquake. This process enhances
46 the transportation of Radon from its original enclosure following the cracks into the
47 atmosphere. Significant radon concentration anomalies were also observed prior to the
48 Uttarkashi earthquake of 20th October, 1991; $m_b \sim 6.5$ (Virk and Singh, 1994).

49 North-East India (NE India) is highly vulnerable to earthquake and lies in seismic zone
50 V (BIS 2002) and frequent occurrence of earthquake facilitates the probability of finding
51 precursory phenomena which may lead to a successful prediction in near future. With this



52 objective a Multiparametric Geophysical Observatory (MPGO) in Ouguri Hills (Latitude
53 26.61°; Longitude 92.78°, Elevation~82m), Tezpur, Assam, India with the installation of
54 several geophysical instruments collecting data simultaneously, portray an opportunity towards
55 identification of precursory signatures prior to earthquakes. Earthquake precursory and
56 prediction studies advanced in late 1970s and Heicheng earthquake of 4th February is a land-
57 mark which was in short-term successfully predicted in 1975 in China (Adams, 1976). The
58 accomplished medium term forecast of M~7.5 earthquake on 6th August, 1988 in northeast
59 Indian region (Gupta and Singh, 1988) encouraged to strengthen such studies in India. Another
60 successful short term prediction was done of ($M \geq 4$) in Koyna region of western India, famous
61 for Reservoir Triggered Seismicity (Verma and Bansal, 2012).

62 The study tries to correlate radon emanation in soil gas with earthquakes within the
63 epicentral distance of 100 km of mb > 3.1 from MPGO, Tezpur which is situated in a highly
64 tectonically strained and seismically active region. The major problem arises is the removal of
65 quasi periodic, diurnal (mostly due to temperature) and semidiurnal (mostly due to pressure)
66 components (Kumar et al., 2015). Radon anomalies are governed by seismic activity as well as
67 by meteorological parameters (soil temperature, pressure, rainfall, moisture and even wind for
68 atmospheric radon; Stranden et al., 1984; Kumar et al., 2009;Walia et al., 2005) which in turn
69 makes it more complex for identifying the seismic induced anomalies. Here in the investigation
70 characteristics features of temporal soil radon concentrations variability at MPGO, Tezpur is
71 scrutinized by applying singular spectrum analysis (SSA) in concern to the objective of filtering
72 the meteorological parameters on radon emanation. SSA is a relatively innovative and powerful
73 advanced method which has been used across many applied problems for different scientific
74 fields (e.g., Fraedrich, 1986, Serita et al., 2005). The foremost concept of SSA is applying PCA
75 on trajectory matrix acquired from the original time series following time series reconstruction.

76



77 **2 Seismotectonics of the region**

78 In middle of the active Kopili and Bomdila fault, the MPGO is situated. The Kopili
79 and Bomdila faults comprise Neogene-Quaternary sediments, which directly were deposited
80 over the Archean basement. The Kopili fault zone in an approx is 100 km in width and 300 km
81 in length. It is a NW-SE trending strike-slip fault (Kayal et al., 2006, Bhattacharya et al., 2008,
82 2010). The two Precambrian massifs - the Shillong Plateau and the Mikir Hills is delineated by
83 the tectonic disposition of the Kopili fault. MPGO is bounded to the north by the Main
84 Boundary Thrust (MBT) and to the south by the NE-SW trending Belt of Schuppen (Figure 1).
85 The Bomdila fault is strike slip fault of about 400 km in length which trends along WNW-ESE
86 direction. The northern portion of the fault mostly lies in the Gondwana, Paleogene and
87 Neogene sediments. This fault is surrounded by the Belt of Schuppen to the east and south by
88 the Mikir massif and to the west. The fault cuts across the Himalayan fold belt towards the
89 north (Nandy and Dasgupta, 1991).

90 The Kopili Fault has produced two large earthquakes (Figure 1) $M_w \sim 7.7$, 1869 event
91 (Figure 1) in the south eastern edge of the fault contravening the Naga-Disang thrust and
92 $M_w \sim 7.2$, 1943 earthquake which occurred farther to the north of 1869 event within a period of
93 nearly 75 years (Kayal, 2008). It is highly active with strong seismicity discernible down up to
94 depth of about 50 km, and which extends to the Main Central Thrust (MCT) in the Bhutan
95 Himalaya. Even if MCT is dormant (Ni and Barazangi, 1984), intense activity is observed at
96 the region where Kopili Fault meets the MBT and MCT (Nandy, 2001, Kayal et al., 2010,
97 2012). This is demonstrated by the August 19, 2009 Earthquake ($M_w \sim 5.1$) in the Assam Valley
98 that occurred in the center of the Kopili fault zone and the September 21, 2009 strong Bhutan
99 Himalaya Earthquake ($M_w \sim 6.3$) that occurred at the northern end of the Kopili fault where it
100 connects with the MCT (Kayal et al., 2012). Both the earthquakes are shallow focus (depth ~
101 10 km) showing right lateral strike-slip faulting (Kayal et al., 2010) which suggests that the



102 Kopili fault zone is experiencing compressional stress due to the Indo-Burma arc and Himalyan
103 arc to the east and the north respectively which is characterized by transverse tectonics. The
104 Bomdila Fault inter-weaves across three major tectonic domains of the NE-India, namely
105 MCT, MBT and Naga-Disang thrust along NW-SE direction. The earthquake events along
106 Bomdila fault occur in a diffused pattern having post-collisional intracratonic characteristics
107 (Nandy and Dasgupta, 1991). It is observed that, the Upper Brahmaputra Valley stretching
108 between the Bomdila Fault and almost near NW-trending Mishmi Thrust in the northeast is
109 seismically dormant, and is recognized as the Assam Gap (Khattri, 1983).

110 **3 Method and techniques**

111 **3.1 Soil radon (Rn-222) time series**

112 A BMC2 barasol manufactured by Algade is into operation for soil radon emanation
113 time series data in MPMGO for earthquake prediction and precursory studies. Soil gas radon
114 emanation every 15 minutes is being continuously monitored. The barasol probe is kept fitted
115 inside a plastic tube (length 1.5m and diameter of 0.0635m) with open bottom dug inside the
116 ground in such a way that the detection unit (detector sensitivity-0.02 pulses/h for 1 Bq/m³ and
117 saturation volumetric activity-3MBq/ m³) which is at the bottom of the probe lies 1m from the
118 ground level. A silicon alpha detector detects the radon gas which enters the detection chamber
119 when it emanates from the soil. The radon pass in a detection volume over three cellulose filters
120 which allows to trap all the solid daughter products of radon. The sensor is a fixed silicon
121 detector with a depleted depth of 100µm and 400 mm² of sensitive area. It performs the
122 counting by atomic spectrometry of radon (Rn-222) and daughter products created in the
123 detection volume (with window customized between 1.5 MeV and 6 MeV). The probe system
124 is embedded with soil pressure and temperature sensor. The sensor calibration permits the
125 volumic activity of the radon (Rn-222) to be evaluated. In the present investigation the soil



126 radon emanation temporal variability at MPGO, Tezpur the radon data were prudently checked
127 for no gaps or discontinuous jump. Digital filter (Butterworth) is applied to eliminate the high
128 frequency quasi periodic components from the soil radon time series for better discernibility of
129 seismic induced anomalies.

130 3.2 Singular Spectrum Analysis

131 The SSA results and graphs in the investigation are acquired by using Caterpillar-SSA
132 3.40 software (Alexandrov and Golyandina, 2004). Window selection rule applied to the time
133 series is one half of the length of the time series to meet the theoretical requirements for the
134 investigation (Golyandina, 2010, Khan, 2011, Hassani, 2007). The singular value
135 decomposition (SVD) algorithm was applied as it is more accurate than QR iteration which
136 are the common most algorithm for solving of eigenvalues and singular value problems
137 (Demmel, 1992). The main objective of SSA is decomposing the original time series into sum
138 of series such that each of the component in this sum can be known (either as a trend, periodic
139 or quasi-periodic components) or noise. This is accomplished by decomposition and
140 reconstruction. At the first the time series is decomposed following the reconstruction of the
141 original time series (which is without noise). The methodology adopted here is first to
142 embedding a 1-dimension time series say, $Y_T = (y_1, \dots, y_T)$ into a multi-dimensional time series
143 X_1, \dots, X_K having vectors $X_i = (y_i, \dots, y_{i+L-1}) \in R^L$ (Golyandina et al., 2001, 2001). Here the value
144 of $K = T - L + 1$. The X_i Vectors are called L -lagged vectors. The embedding depends on the
145 window length L , such that $2 \leq L \leq T$ which results for trajectory matrix (Hankel matrix:
146 diagonal elements $i + j = \text{const.}$ are equal) $X = [X_1, \dots, X_K] = (X_{ij})_{i,j=1}^{L,K}$. Secondly the Singular
147 Value Decomposition (SVD) of the trajectory matrix is performed to represent it as an addition
148 of bi-orthogonal elementary matrices having rank one. Represented by $\lambda_1, \dots, \lambda_L$ which are the
149 Eigen-values of XX' in a descending order of magnitude ($\lambda_1 \geq \dots \lambda_L \geq 0$) and by U_1, \dots, U_L which



150 are the orthonormal system (i.e. $U_i, U_j = 0$ for $i \neq j$) is the orthogonality property) and $\|U_i\|=1$,
151 of the eigenvectors of the matrix XX' corresponding to these eigenvalues. (U_i, U_j) is the inner
152 product of the vectors U_i and U_j and $\|U_i\|$ is the norm of the vector U_i . The Set

$$153 \quad d = \max (i, \text{ such that } \lambda_i > 0) = \text{rank } X \quad (\text{I})$$

154 If we represent $V_i = X' U_i / \sqrt{\lambda_i}$, then SVD of the trajectory matrix can be represented
155 as:

$$156 \quad X = X_1 + \dots + X_d \quad (\text{II})$$

157 Here $X_i = \sqrt{\lambda_i} U_i V_i'$ ($i = 1, \dots, d$).

158 Thirdly the series reconstruction is accomplished by grouping, to split the elementary
159 matrices (X_i) into various groups and addition of the matrices within each and every group. Say
160 $I = \{i_1, \dots, i_p\}$ be group of indices i_1, \dots, i_p . Then X_I matrix parallel to the group I is defined as X_I
161 $= X_{i_1} + \dots + X_{i_p}$. Splitting the set of indices $J = 1, \dots, d$ in disjoint subsets I_1, \dots, I_m can be
162 representation as:

$$163 \quad X = X_{I_1} + \dots + X_{I_m} \quad (\text{III})$$

164 The eigentriple grouping is the process of choosing the sets I_1, \dots, I_m . Finally diagonally
165 averaging transfers each I matrix into a time series, which is an additive component of the
166 initial series Y_T . If z_{ij} is an element of the matrix Z . Then k -th term of the produced series is
167 acquired by averaging z_{ij} for i, j such that $i + j = k + 2$. This procedure is known as diagonal
168 averaging (Hankelization) of the matrix Z . The Hankelization of a matrix Z is the Hankel matrix
169 HZ which is the trajectory matrix corresponding to the series obtained from diagonal averaging.
170 Hankelization is a best logical technique that HZ matrix is the nearest to Z among all



171 corresponding size of Hankel matrices (Golyandina et al., 2001). Now applying the
172 Hankelization technique to each and every matrix components in equation III, we get

$$173 \quad X = \tilde{X}_{I_1} + \dots + \tilde{X}_{I_m} \quad (IV)$$

174 Here $X_{II} = HX$ corresponding to initial series $Y_T = (y_1, \dots, y_T)$ decomposition into a
175 sum of m series as

$$176 \quad y_t = \sum_{k=1}^m \tilde{y}_t^{(k)} \quad (V)$$

177 Here $\tilde{y}_t^{(k)} = y_1^{(k)} + \dots + y_T^{(k)}$ corresponds matrix X_{I_j} .

178 **4 Results**

179 The average value of radon for a period of six month from April 2017-September 2017
180 was found to be in the range 55-117 kBq/m³. The average emanation of soil-gas radon at
181 MPGO for April, May, June, July, August and September 2017 is reported to be 55.94, 93.11,
182 109.12, 117.69, 101.45, 92.34 (kBq/m³) respectively with standard deviation (Std.) of 21.3,
183 28.53, 19.07, 28.09, 25.86, 18.65 (kBq /m³) respectively. Simultaneously variation of soil
184 temperature and pressure with radon emanation was observed. Usually, radon shows positive
185 correlation with temperature i.e. the soil radon concentration increases with increase in
186 temperature and decreases as temperature decrease. The correlation coefficient (Pearson
187 correlation) between radon and temperature is found to be 0.5 signifying positive correlation,
188 while the correlation coefficient between radon and pressure is found to be -0.5 signifying
189 negative correlation with an average temperature and pressure of 28.60 °C and 991.03 mbar
190 respectively during afore mentioned period. The positive correlation of radon with temperature
191 might be due to the rise in diffusion rate with temperature (Sharma et al. 2000, Singh et al.
192 2008). The negative correlation coefficient was found for soil radon and pressure which signify,
193 with the increase in pressure, the radon emanation decreases while with the decrease in pressure



194 the radon emanation increases. In general, the negative correlation is due to the diffusion
195 process which slows down with increase in pressure, which in turn decreases the radon
196 concentration in the soil. The average value of pressure, temperature, standard deviation,
197 percentage (%) correlation coefficient for the observation period is detailed in Table 1. The
198 maximum and minimum temperature observed was 31.24 °C and 23.78 °C i.e. a change of 7.46
199 °C during the period of observation. Simultaneously, the maximum and minimum pressure
200 during the period of observation was 999.32 mbar and 980.72 mbar i.e. a change of 18.6 mbar.
201 Digital filter (Butterworth) is applied to eliminate the high frequency quasi periodic
202 components from the soil radon time series for better discernibility of seismic induced
203 anomalies and is represented in Figure 2.

204 The covariance matrix of the first 9 group of soil radon (Rn-222) time series is
205 represented in Figure 3. The singular value decomposition (SVD) to Rn-222 data evinced that
206 first 9 eigenfunctions (Figure 4) when grouped resulted for 99.90 % of the total variance in the
207 individual time series. The eigenfunction group 1 and 2 represents the aperiodic component and
208 group 3 to 9 represented periodic components. The periodic and aperiodic component mostly
209 corresponds to diurnal and semidiurnal variation (Kumar et al., 2015). The decomposed
210 eigenvectors in soil radon time series is grouped into two classes as diurnal and semidiurnal
211 variation. The sum of eigenfunction group 1 and 2 accounts for 98.62 % and group 3 to 9
212 accounts for 0.48 % of the variance. Radon variations is governed by daily variations, which
213 accounts to 99.90 % of the total variance in soil gas radon at the MPGO, Tezpur. The Principal
214 Component of soil radon (Rn-222) related to the first 9 grouping of eigentriples is represented
215 in Figure 5 and w-correlation matrix for the 9 reconstructed components is represented in
216 Figure 6.

217 The covariance matrix of the first 9 group of soil temperature and pressure time series
218 is represented in Figure 7 and Figure 11 respectively. The decomposed eigenfunctions for soil



219 temperature and pressure time series by applying SSA is represented in Figure 8 and Figure 12
220 respectively. The first 9 eigenfunction group from SVD to atmospheric temperature records
221 accounts nearly about 99.99 % and first 9 eigenfunction group of soil pressure 100 % of the
222 variation respectively. It is discernible that first eigenfunction 1 alone itself is capable of
223 producing 100 % variation but the time series is well modeled when first 9 eigenfunction is
224 grouped. This evinces SVD to radon, soil temperature and soil pressure data evince that first
225 9 eigenfunction accounts >98.00 % of the variance of the individual data series. This is
226 fascinating to observe that sum of first 9 eigenfunction is fairly sufficient to reproduce the
227 prominent features of the overall variation. This also suggests that the most significantly
228 produced variations are mostly free from naturally induced variations. Soil pressure variations
229 are dominated by semidiurnal variations by 100 % of the total variation in atmospheric pressure
230 at MPGO, Tezpur. On the other hand soil temperature variations is dominated by daily
231 variations like radon variation which account to 97.99 % whereas soil pressure accounts for
232 100 % of the total variance. This suggest that daily variations of soil radon (Rn-222) emanation
233 are controlled by soil pressure in MPGO, Tezpur during the investigation period followed by
234 soil temperature. The Principal Component of soil temperature related to the first 9 grouping
235 of eigentriples is represented in Figure 9 and w-correlation matrix for the 9 reconstructed
236 components is represented in Figure 10. The Principal Component of soil pressure related to
237 the first 9 grouping of eigentriples is represented in Figure 13 and w-correlation matrix for the
238 9 reconstructed components is represented in Figure 14. The reconstructed time series for soil
239 radon (Rn-222), temperature and pressure is represented is Figure 15 and it's residual in Figure
240 16. It is also discernible that the during the investigation time period the pressure change was
241 more than temperature change which also evinces the variation of soil radon at MPGO, Tezpur
242 was more governed by pressure followed by temperature change. The quasi periodic, diurnal
243 (periodic mostly due to temperature) and semidiurnal (aperiodic mostly due to pressure) were



244 eliminated by Singular Spectrum Analysis in the reconstructed time series by grouping and
245 analyzing the eigenfunctions and principle component of individual time series of Rn-222,
246 temperature and pressure respectively. The soil pressure and temperature were found to be
247 negatively correlated to each other (-0.62) which produces a pseudo effect in the soil radon
248 time series. The grouping and reconstruction of the time series also eliminates these pseudo
249 effect arising due soil pressure and temperature.

250 **5 Discussion**

251 The reconstructed soil radon time series along with the seismic activity during the
252 investigation period is shown in Figure 17. The hypocentral parameters of the earthquake
253 events found to have correlation with soil radon emanation is listed in Table 2. It was observed
254 that there were certain positive amplitude rise anomalies in radon emanation prior to six out of
255 9 earthquakes which occurred in the vicinity (100 km radially from MPMO, Tezpur). Increase
256 in the soil radon concentration is generally assigned to developments of microcracks, fractures
257 and fissure caused by dilatancy prior to earthquake. This process enhances the transportation
258 of radon from its original enclosure following the cracks. The rise in soil radon concentration
259 prior to an earthquake may be due to the strain buildup processes in the area. During this
260 process, very small fractures are developed in the rocks which enhances the contribution of
261 radon gas to the soil near the surface of earth (Miklavčič et al., 2008). Three earthquake events
262 were preceded by negative anomalies. The negative anomalies might be due to the
263 circumstance that during the final stage of dilatancy model prior to an earthquake the Rn-222
264 emanation can be stable or it can decrease (Tomer, 2016). This is because, during the final
265 stage prior an earthquake, rupture occurs and fluid pressure and stress on rocks is released
266 (Bakhmutov and Groza, 2008). The fluid pressure increases resulting in water level rise and
267 this does not allow the soil gas Rn-222 to escape from the surface which in turn reduces or
268 stabilizes the emanation of Rn-222. Further a decreasing radon anomaly as observed in this



269 study may be the result of squeezing effect of compressional stress built up in the rock, which
270 in turn result in soil porosity changes at micro scale. There were certain events which occurred
271 on the same day or just a very short seismic gap of 1 or 2 days. Here in the case earthquake
272 with higher magnitude might also be the probable reason for the anomalous behavior of the
273 soil gas radon emanation, as for spatio-temporal clustered earthquakes, the largest magnitude
274 earthquake is presumed to precede the anomalies in radon emanation (Hartmann and Leavy,
275 2005). Positive as well as negative anomalies were observed prior to 9 events which occurred
276 in the vicinity (100 km radially from MPGO) with in a short span of time.

277 **6 Conclusion**

278 The investigation concludes that digital filter assists in eliminating the high frequency
279 quasi periodic components from the time series. The SSA method helps eliminating the diurnal
280 and semidiurnal fluctuations from soil radon time series for improved correlating and detection
281 of the soil radon emanation with seismic activity. The investigation also evinced that radon is
282 dominated by daily variation at MPGO, Tezpur and is controlled by soil pressure followed by
283 temperature. It is also concluded that principle component analysis helps in removing the
284 pseudo effect pertaining to simultaneous soil pressure and temperature effect. It was observed
285 that there were certain positive amplitude rise anomalies in radon emanation prior to six events
286 out of 9 earthquakes which occurred in the vicinity (100 km radially from MPGO, Tezpur)
287 within a short span of time. The increase of radon emanation with temperature might be the
288 result of increasing diffusion rate with temperature. Three earthquake events were preceded by
289 negative anomalies. The negative anomalies might be due to the circumstance that during the
290 final stage of dilatency model prior to an earthquake the soil gas radon emanation can be stable
291 or it can decrease. This is because, during the final stage prior an earthquake, rupture occurs
292 and fluid pressure and stress on rocks is released. Further a decreasing radon anomaly as



293 observed in this study may be the result of squeezing effect of compressional stress built up in
294 rock, which in turn changes porosity of soil at micro scale.

295 **Acknowledgements.** We acknowledge our sincere thanks to Ministry of Earth Sciences
296 (MoES) Government of India for providing funds vide project no.MoES/P.O.(Seismo)/NPEP-
297 16/2011. We thank Director, CSIR-NEIST Jorhat for giving necessary permission to publish
298 this paper.

299 **References**

300 Adams, R. D.: The Haicheng, China, earthquake of 4 February 1975; the first successfully
301 predicted major earthquake, *Earthquake Engineering & Structural Dynamics*, 4, 423-
302 437, 1976.

303 Alexandrov, T., and Golyandina, N.: The automatic extraction of time series trend and
304 periodical components with the help of the Caterpillar-SSA approach, *Exponenta Pro*,
305 3, 54-61, 2004.

306 Bakhmutov, V., and Groza, A.: The dilatancy-diffusion model: new prospects, *Proceedings*,
307 *International Conference: Problems of Geocosmos*, 7th, St. Petersburg, Russia, May,
308 2008, 26-30.

309 Bhattacharya, P. M., Kayal, J., Baruah, S., and Arefiev, S.: Earthquake source zones in
310 northeast India: seismic tomography, fractal dimension and b value mapping, in:
311 *Seismogenesis and Earthquake Forecasting: The Frank Evison Volume II*, Springer,
312 145-158, 2010.

313 Bhattacharya, P. M., Mukhopadhyay, S., Majumdar, R., and Kayal, J.: 3-D seismic structure
314 of the northeast India region and its implications for local and regional tectonics,
315 *Journal of Asian Earth Sciences*, 33, 25-41, 2008.

316 Demmel, J., and Veselić, K.: Jacobi's method is more accurate than QR, *SIAM Journal on*
317 *Matrix Analysis and Applications*, 13, 1204-1245, 1992.

318 Fraedrich, K.: Estimating the dimensions of weather and climate attractors, *Journal of the*
319 *atmospheric sciences*, 43, 419-432, 1986.

320 Golyandina, N., Nekrutkin, V., and Solntsev, V.: „Caterpillar“-SSA Technique for Analysis of
321 Time Series in Economics, *New Models of Business: Managerial Aspects and Enabling*
322 *Technology*, 198, 2001.

323 Golyandina, N., Nekrutkin, V., and Zhigljavsky, A. A.: *Analysis of time series structure: SSA*
324 *and related techniques*, Chapman and Hall/CRC, 2001.

325 Golyandina, N.: On the choice of parameters in singular spectrum analysis and related
326 subspace-based methods, arXiv preprint arXiv:1005.4374, 2010.

327 Gupta, H.: Medium-term earthquake prediction, *Eos, Transactions American Geophysical*
328 *Union*, 69, 1620-1630, 1988.



- 329 Hartmann, J., and Levy, J. K.: Hydrogeological and gasgeochemical earthquake precursors—A
330 review for application, *Natural Hazards*, 34, 279-304, 2005.
- 331 Hassani, H.: *Singular spectrum analysis: methodology and comparison*, 2007.
- 332 Kayal, J., Arefiev, S. S., Baruah, S., Tatevossian, R., Gogoi, N., Sanoujam, M., Gautam, J.,
333 Hazarika, D., and Borah, D.: The 2009 Bhutan and Assam felt earthquakes (Mw 6.3
334 and 5.1) at the Kopili fault in the northeast Himalaya region, *Geomatics, Natural
335 Hazards and Risk*, 1, 273-281, 2010.
- 336 Kayal, J., Arefiev, S., Barua, S., Hazarika, D., Gogoi, N., Kumar, A., Chowdhury, S., and
337 Kalita, S.: Shillong plateau earthquakes in northeast India region: complex tectonic
338 model, *CURRENT SCIENCE-BANGALORE-*, 91, 109, 2006.
- 339 Kayal, J., Arefiev, S., Baruah, S., Hazarika, D., Gogoi, N., Gautam, J., Baruah, S., Dorbath, C.,
340 and Tatevossian, R.: Large and great earthquakes in the Shillong plateau—Assam valley
341 area of Northeast India Region: Pop-up and transverse tectonics, *Tectonophysics*, 532,
342 186-192, 2012.
- 343 Kayal, J.: *Microearthquake seismology and seismotectonics of South Asia*, Springer Science
344 & Business Media, 2008.
- 345 Khan, M. A. R., and Poskitt, D.: Window length selection and signal-noise separation and
346 reconstruction in singular spectrum analysis, *Monash Econometrics and Business
347 Statistics Working Papers*, 23, 2011-2023, 2011.
- 348 Khattri, K., and Tyagi, A.: Seismicity patterns in the Himalayan plate boundary and
349 identification of the areas of high seismic potential, *Tectonophysics*, 96, 281-297, 1983.
- 350 Kumar, A., Walia, V., Arora, B. R., Yang, T. F., Lin, S.-J., Fu, C.-C., Chen, C.-H., and Wen,
351 K.-L.: Identifications and removal of diurnal and semidiurnal variations in radon time
352 series data of Hsinhua monitoring station in SW Taiwan using singular spectrum
353 analysis, *Natural Hazards*, 79, 317-330, 2015.
- 354 Miklavčić, I., Radolić, V., Vuković, B., Poje, M., Varga, M., Stanić, D., and Planinić, J.: Radon
355 anomaly in soil gas as an earthquake precursor, *Applied radiation and isotopes*, 66,
356 1459-1466, 2008.
- 357 Nandy, D., and Dasgupta, S.: Seismotectonic domains of northeastern India and adjacent areas,
358 *Physics and Chemistry of the Earth*, 18, 371-384, 1991.
- 359 Nandy, D.: *Geodynamics of Northeastern India and the adjoining region*, ACB publications,
360 2001.
- 361 Ni, J., and Barazangi, M.: Seismotectonics of the Himalayan collision zone: Geometry of the
362 underthrusting Indian plate beneath the Himalaya, *Journal of Geophysical Research:
363 Solid Earth*, 89, 1147-1163, 1984.
- 364 Serita, A., Hattori, K., Yoshino, C., Hayakawa, M., and Isezaki, N.: Principal component
365 analysis and singular spectrum analysis of ULF geomagnetic data associated with
366 earthquakes, *Natural Hazards and Earth System Science*, 5, 685-689, 2005.



- 367 Sharma, A. K., Walia, V., and Virk, H.: Effect of meteorological parameters on radon
368 emanation at Palampur (HP), Journal of Association of Exploration Geophysicists, 21,
369 47-50, 2000.
- 370 Singh, H., Singh, J., Singh, S., and Bajwa, B.: Radon exhalation rate and uranium estimation
371 study of some soil and rock samples from Tusham ring complex, India using SSNTD
372 technique, Radiation Measurements, 43, S459-S462, 2008.
- 373 Singh, S., Kumar, A., Bajwa, B. S., Mahajan, S., Kumar, V., and Dhar, S.: Radon monitoring
374 in soil gas and ground water for earthquake prediction studies in North West Himalayas,
375 India, Terr. Atmos. Ocean. Sci, 21, 685-695, 2010.
- 376 Stranden, E., Kolstad, A., and Lind, B.: The influence of moisture and temperature on radon
377 exhalation, Radiation Protection Dosimetry, 7, 55-58, 1984.
- 378 Stranden, E., Kolstad, A., and Lind, B.: The influence of moisture and temperature on radon
379 exhalation, Radiation Protection Dosimetry, 7, 55-58, 1984.
- 380 Tomer, A.: Radon as a earthquake precursor: a review, Int J Sci Eng Technol, 4, 815-822, 2016.
- 381 Ulomov, V., and Mavashev, B.: The Tashkent Earthquake of 26 April, Tashkent: Acad. Nauk.
382 Uzbeck, 1971.
- 383 Verma, M., and Bansal, B. K.: Earthquake precursory studies in India: Scenario and future
384 perspectives, Journal of Asian Earth Sciences, 54, 1-8, 2012.
- 385 Virk, H., and Singh, B.: Radon recording of Uttarkashi earthquake, Geophysical Research
386 Letters, 21, 737-740, 1994.
- 387 Yang, T., Walia, V., Chyi, L., Fu, C., Chen, C.-H., Liu, T., Song, S., Lee, C., and Lee, M.:
388 Variations of soil radon and thoron concentrations in a fault zone and prospective
389 earthquakes in SW Taiwan, Radiation Measurements, 40, 496-502, 2005.
- 390
- 391
- 392
- 393
- 394
- 395
- 396
- 397
- 398
- 399
- 400
- 401

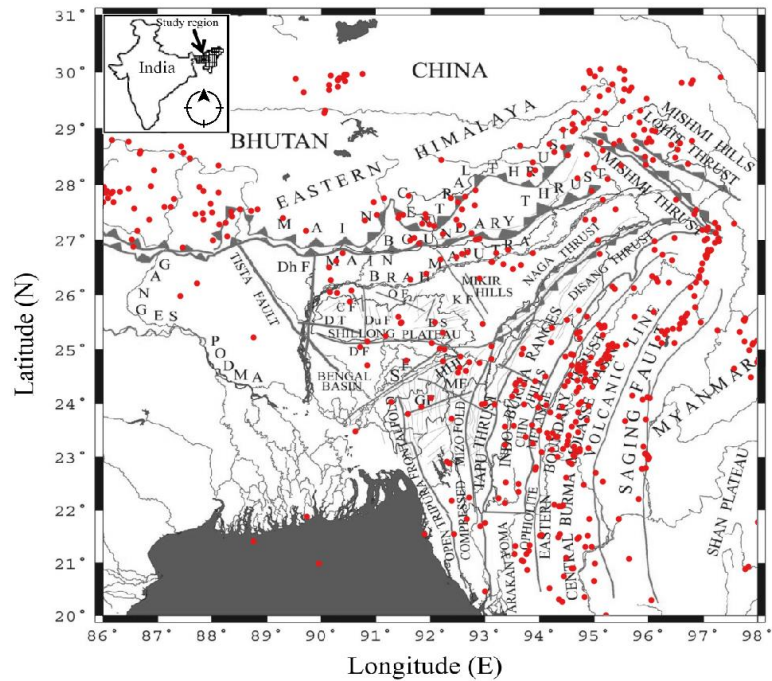


402 **FIGURES AND TABLES**

403

404

405



406

407 **Figure 1:** Map illustrates the earthquake events of $M_w \geq 5$ during 1918 to 2018, in NE-India

408 and its border region (20^0 - 30^0 N and 86^0 - 98^0 E) along with the major tectonic features of the

409 region.

410

411

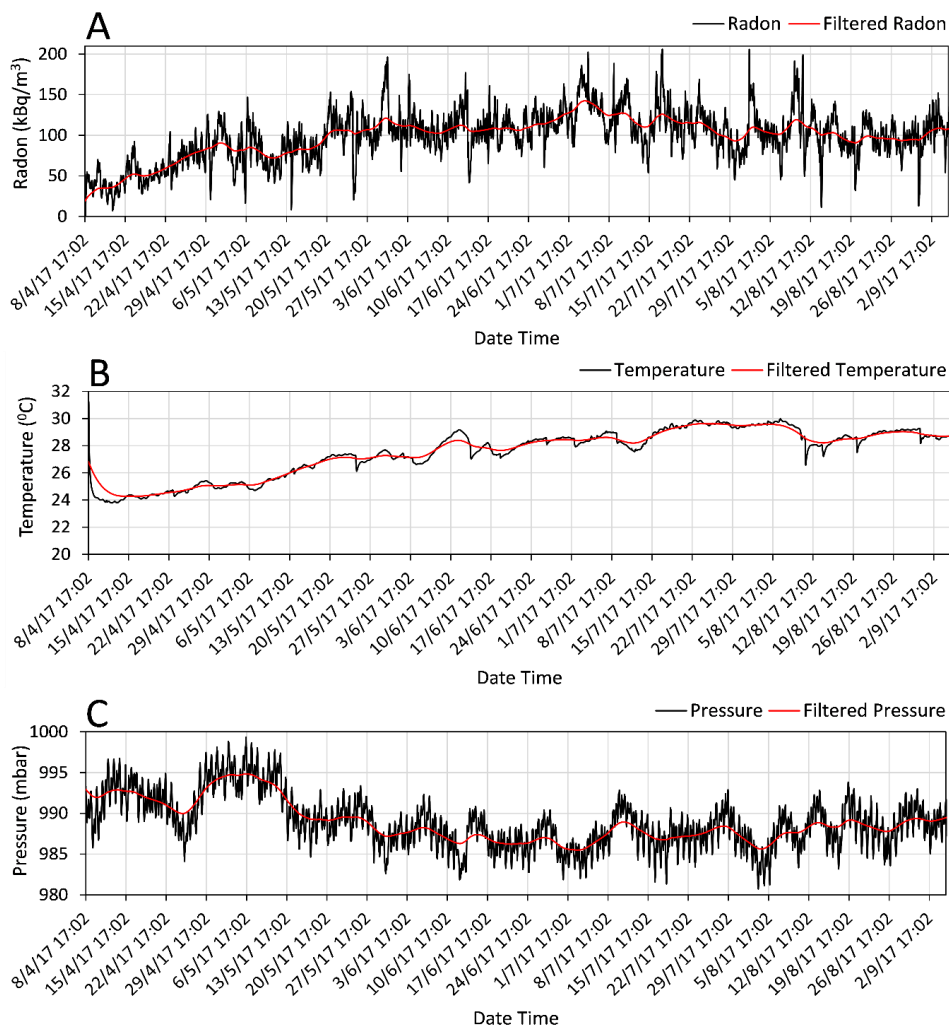
412

413

414

415

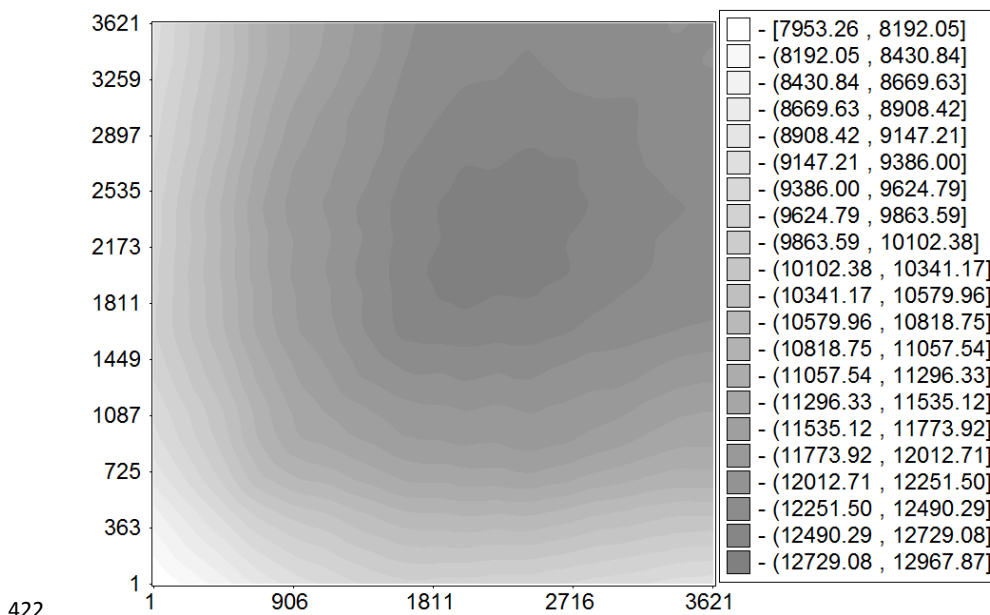
416



417

418 **Figure 2:** The plot represents the removal of high frequency quasi periodic component for A)
419 filtered time series of soil radon, B) filtered time series of soil temperature and C) filtered time
420 series of soil pressure.

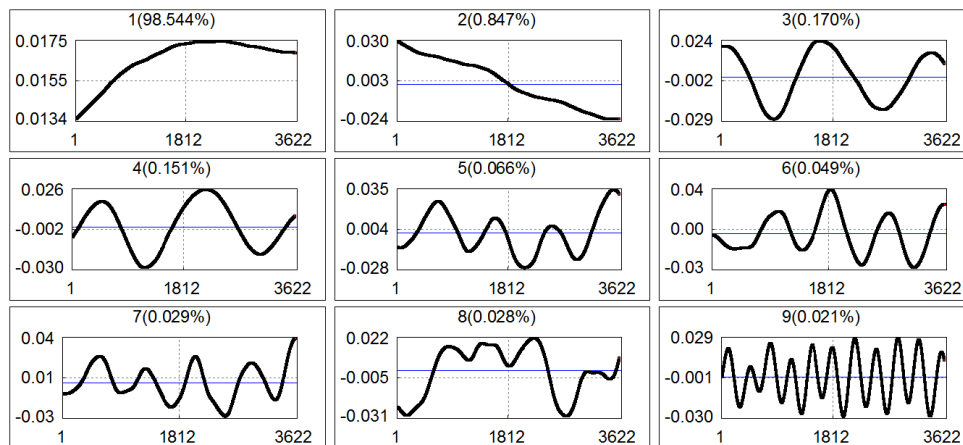
421



422

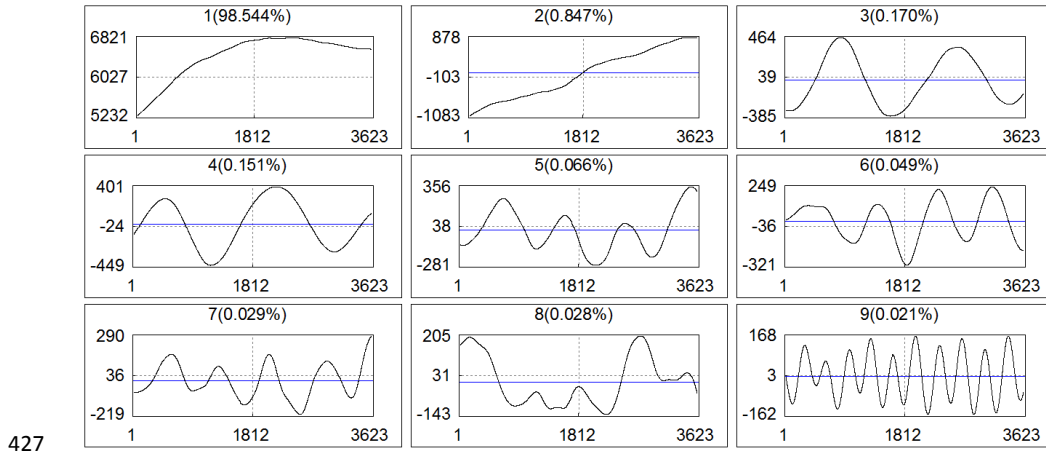
423 **Figure 3:** Covariance matrix of the first 9 group of soil radon (Rn-222) time series.

424



425

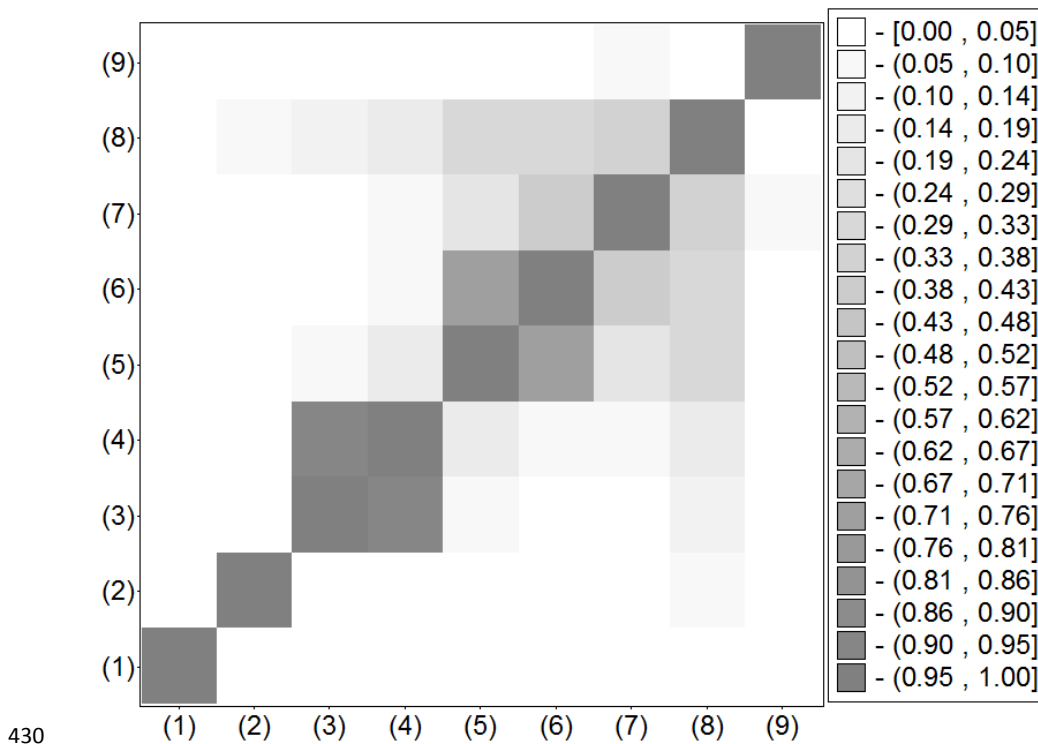
426 **Figure 4:** Eigenfunctions of soil radon (Rn-222) first 9 group.



427

428 **Figure 5:** Principal Component of soil radon (Rn-222) related to the first 9 eigentriples.

429

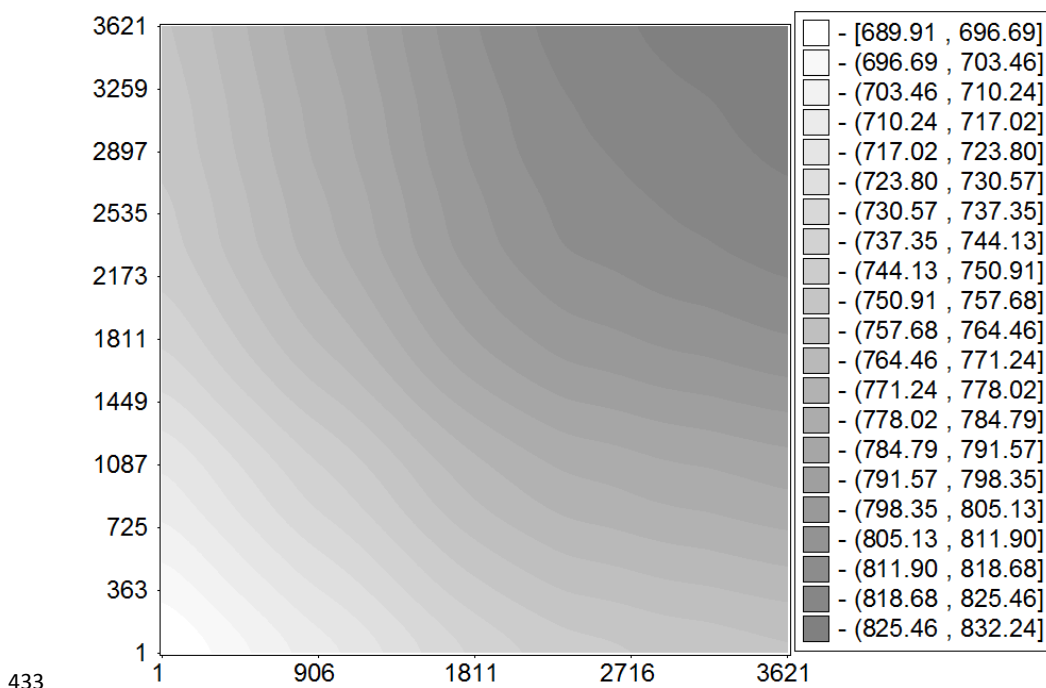


430

431 **Figure 6:** w-correlation matrix for the 9 reconstructed components of soil radon time series.



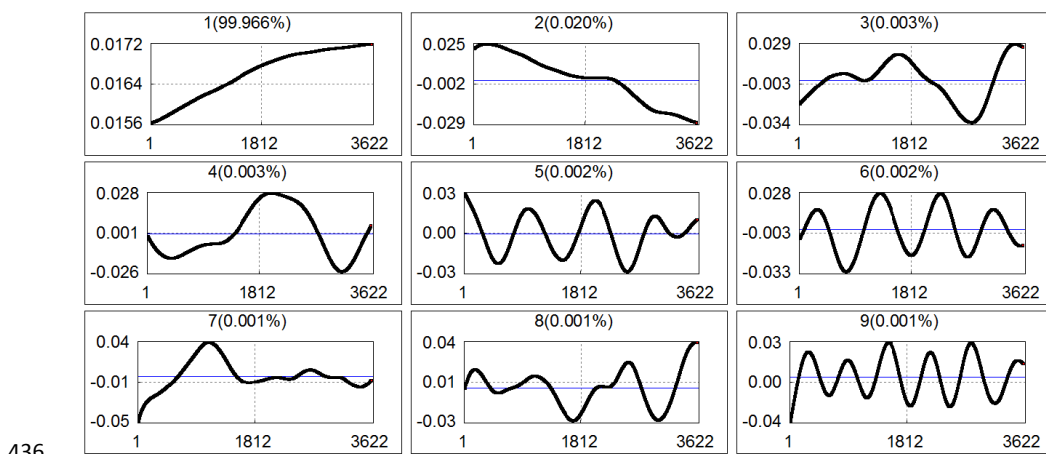
432



433

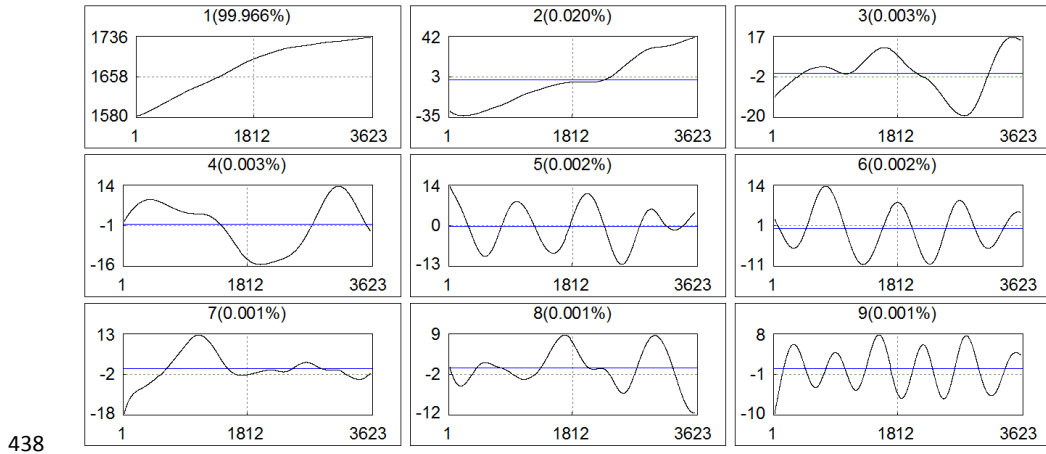
434 **Figure 7:** Covariance matrix of the first 9 group of soil temperature time series.

435



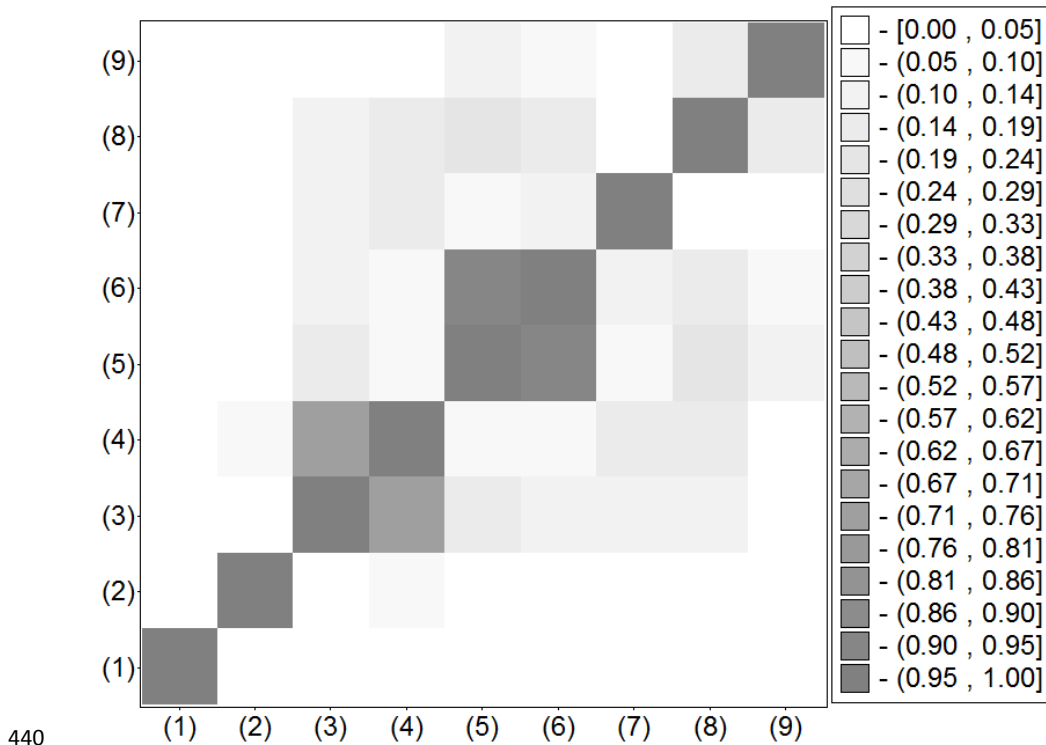
436

437 **Figure 8:** Eigenfunctions of soil temperature first 9 group.



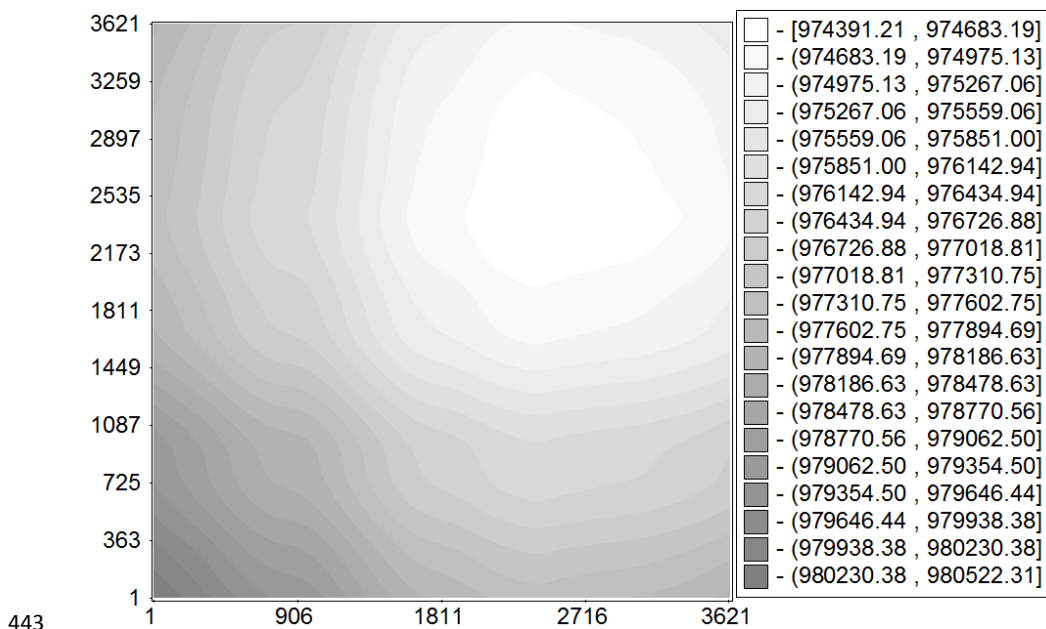
438

439 **Figure 9:** Principal Component of soil temperature related to the first 9 eigentriples.

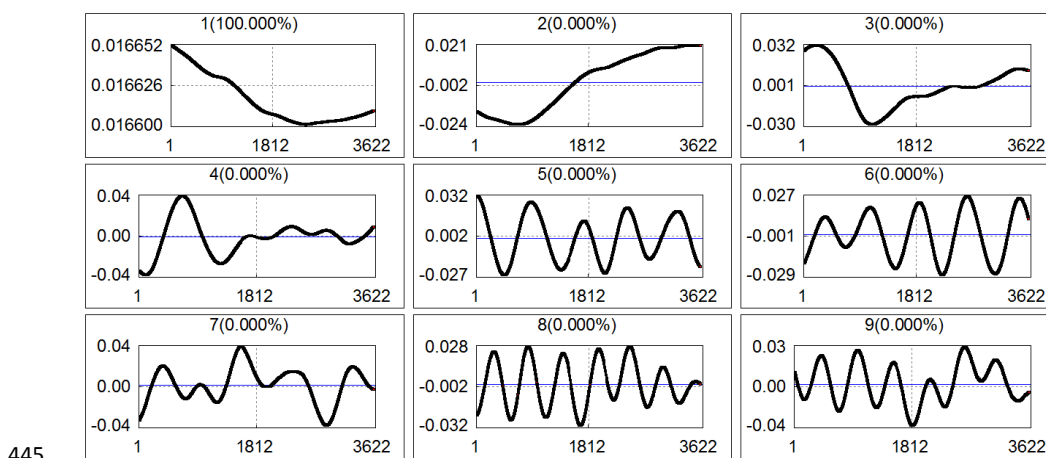


440

441 **Figure 10:** w-Correlation matrix for the 9 reconstructed components of soil temperature time
 442 series.



443 **Figure 11:** Covariance matrix of the first 9 group of soil pressure time series

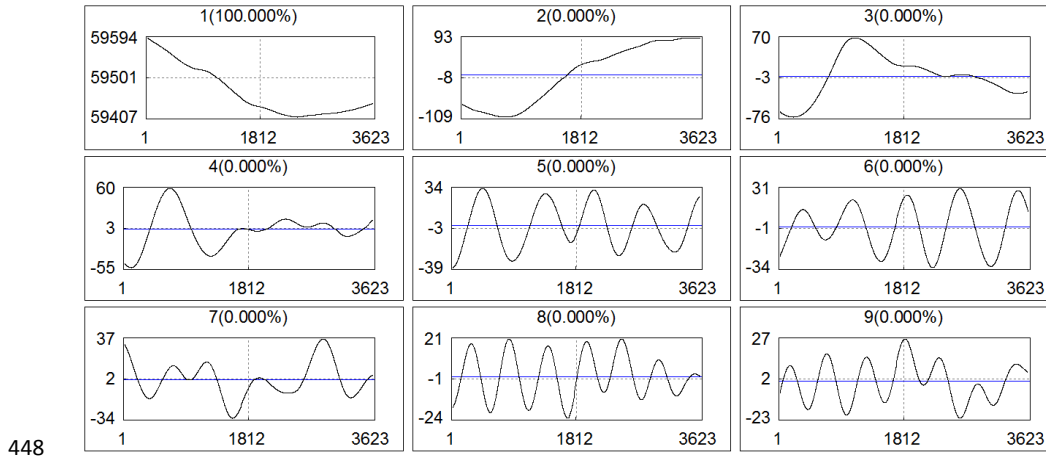


444 **Figure 12:** Eigenfunctions of soil pressure first 9 group.

445

446

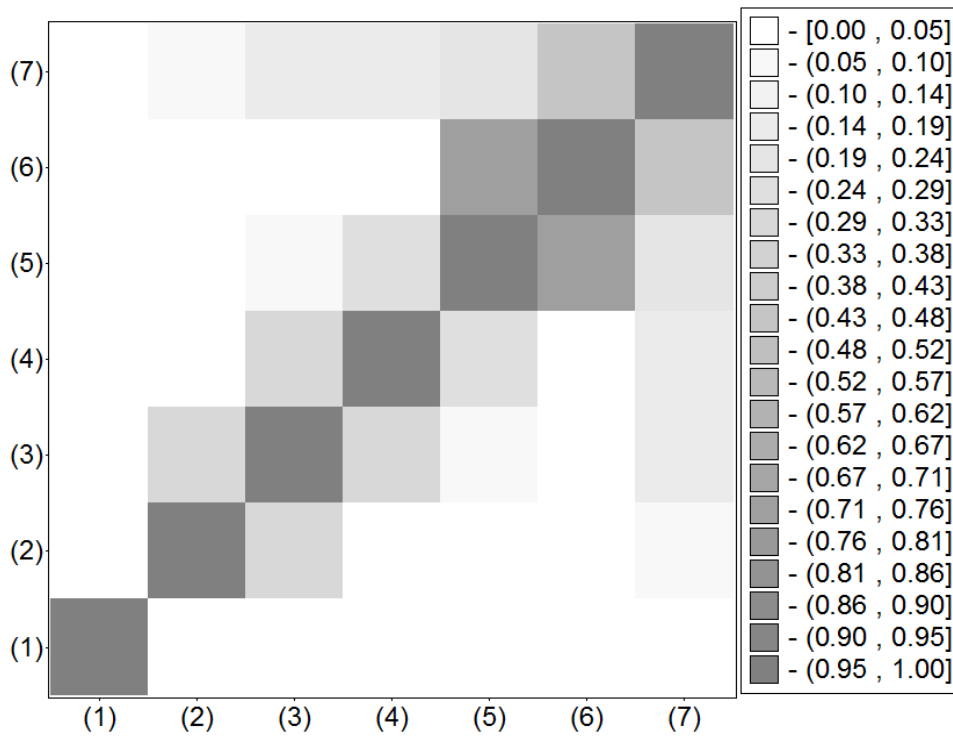
447



448

449 **Figure 13:** of soil temperature related to the first 9 Eigentriples.

450



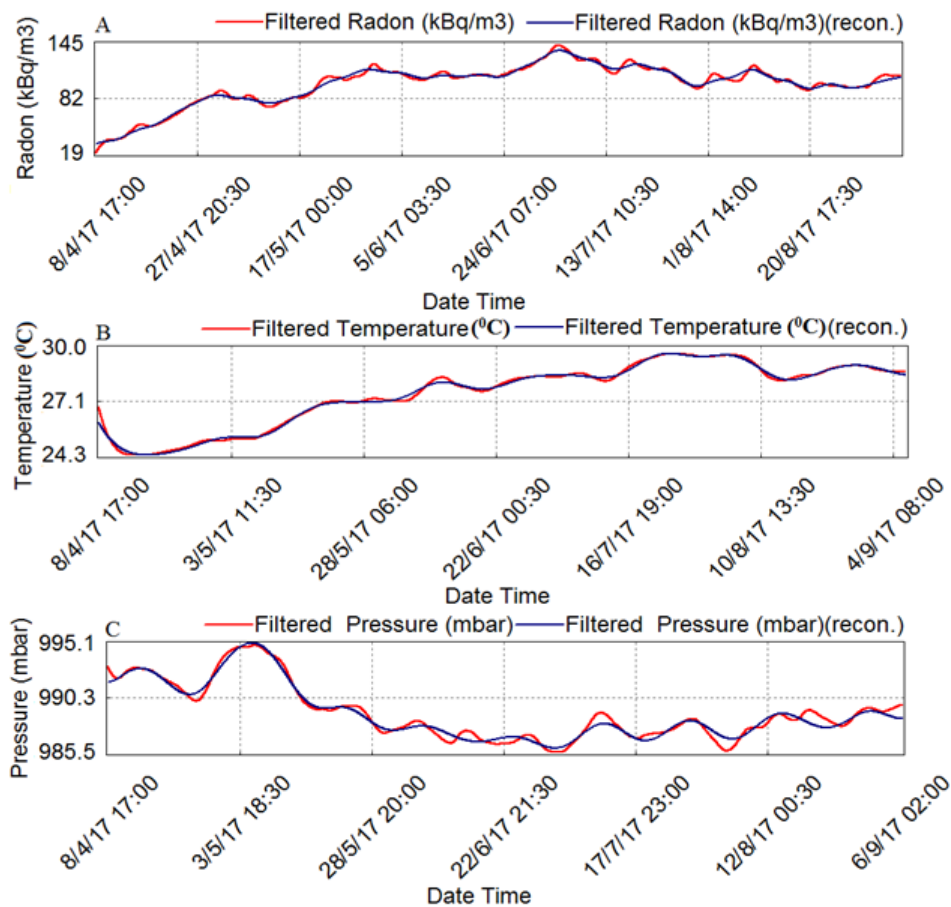
451

452 **Figure 14:** w correlation matrix for the 9 reconstructed components of soil pressure time series.



453

454



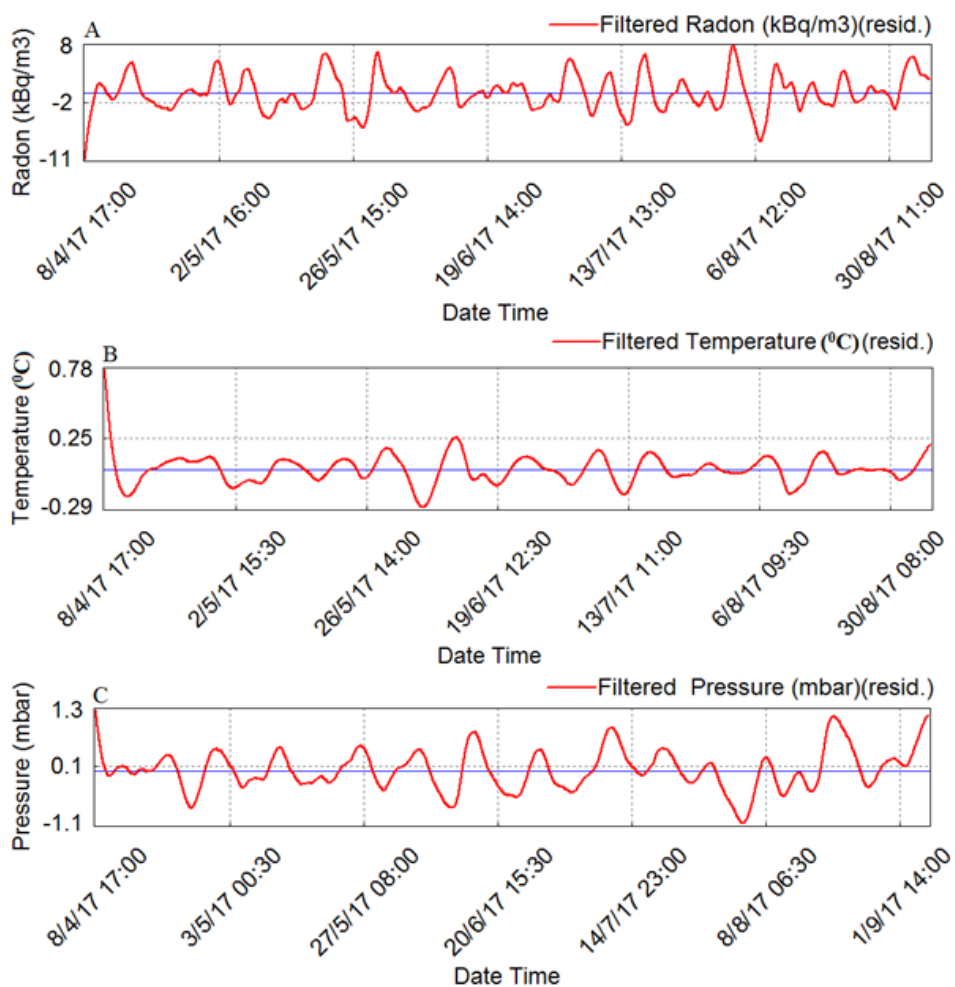
455

456 **Figure 15:** Plot showing the reconstructed time series of A) filtered soil radon, B) filtered
457 temperature and C) filtered pressure.

458

459

460



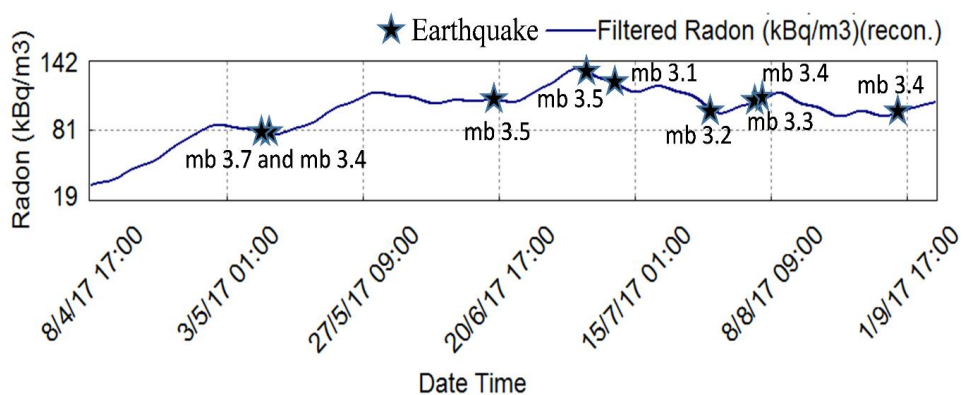
461

462 **Figure 16:** Residual of reconstructed time series of A) Filtered soil radon, B) temperature and
463 C) pressure respectively.

464

465

466



467

468 **Figure 17:** Plot showing the reconstructed filtered time series of soil radon emanation along
469 with earthquake during the investigation period in the vicinity of MPGO, Tezpur (100 km
470 radially from MPGO) which occurred in a very short span of time.

471

472

473

474

475

476

477

478

479

480

481

482

483

484

485

486



487 **Table 1:** The correlation co-efficient of soil radon gas concentration with soil pressure and
488 temperature at OH-MPGO during year 2017.

Parameters	Average (Avg.)	Standard Deviation (Std.)	% Coefficient /Avg.)	Variation (Std. Coefficient	Correlation Coefficient
Radon (KBq/m³)	94.94	23.58	24.84	----	
Temperature (°C)	28.60	0.62	2.19		0.5
Pressure (mbar)	991.03	2.48	0.25		-0.5

489
490
491
492
493
494
495
496
497
498
499
500
501
502
503
504
505
506
507



508 **Table 2:** Hypocentral parameters of the earthquake events found to have correlation with radon
 509 anomaly.

Date of Event	UTC TIME	Lat (°N)	Long (°E)	Place	Depth (km)	Mag (m _b)	Distance from MPGO (km)
09/05/2017	01:53:55	26.3	92.7	Assam	25	3.7	44
09/05/2017	03:26:54	26.6	93.2	Assam	28	3.4	67
20/06/2017	04:31:58	27.1	92.5	West Kameng, Arunachal Pradesh	10	3.5	67
04/07/2017	10:05:47	27.0	92.1	West Kameng, Arunachal Pradesh	10	3.5	78
10/07/2017	23:28:30	27.1	93.8	Papumpare, Arunachal Pradesh	10	3.1	78
25/07/2017	18:28:00	26.3	93.1	Karbi Anglong, Assam	28	3.2	67
05/08/2017	12:24:56	26.8	92.2	Darrang, Assam	10	3.3	44
07/08/2017	11:25:07	26.3	91.7	Kamrup, Assam	10	3.4	100
31/08/2017	17:57:26	26.6	92.7	Sonitpur Assam	10	3.4	67

510
 511
 512
 513
 514
 515